

2014

Advances in the Analysis and Prediction of Turbulent Viscoelastic Flows

T. B. Gatski
Old Dominion University

L. Thais

G. Mompean

Follow this and additional works at: https://digitalcommons.odu.edu/ccpo_pubs

 Part of the [Fluid Dynamics Commons](#)

Repository Citation

Gatski, T. B.; Thais, L.; and Mompean, G., "Advances in the Analysis and Prediction of Turbulent Viscoelastic Flows" (2014). *CCPO Publications*. 183.
https://digitalcommons.odu.edu/ccpo_pubs/183

Original Publication Citation

Gatski, T.B., Thais, L., & Mompean, G. (2014). Advances in the analysis and prediction of turbulent viscoelastic flows. Paper presented at the XXI Fluid Mechanics Conference, Bristol. (*Journal of Physics: Conference Series* 530, pp. 1-14).

Advances In The Analysis And Prediction Of Turbulent Viscoelastic Flows

T B Gatski¹

Center for Coastal Physical Oceanography
and Ocean, Earth and Atmospheric Sciences
Old Dominion University, Norfolk, Virginia 23529 USA

L Thais and G Mompean

Université de Lille Nord de France, USTL, F59000 Lille, and
Laboratoire de Mécanique de Lille, CNRS, UMR 8107,
F59655 Villeneuve d'Ascq, France

E-mail: gatski@ccpo.odu.edu

Abstract. It has been well-known for over six decades that the addition of minute amounts of long polymer chains to organic solvents, or water, can lead to significant turbulent drag reduction. This discovery has had many practical applications such as in pipeline fluid transport, oil well operations, vehicle design and submersible vehicle projectiles, and more recently arteriosclerosis treatment. However, it has only been the last twenty-five years that the full utilization of direct numerical simulation of such turbulent viscoelastic flows has been achieved. The unique characteristics of viscoelastic fluid flow are dictated by the nonlinear differential relationship between the flow strain rate field and the extra-stress induced by the additive polymer. A primary motivation for the analysis of these turbulent fluid flows is the understanding of the effect on the dynamic transfer of energy in the turbulent flow due to the presence of the extra-stress field induced by the presence of the viscoelastic polymer chain. Such analyses now utilize direct numerical simulation data of fully developed channel flow for the FENE-P (Finite Extendable Nonlinear Elastic – Peterlin) fluid model. Such multi-scale dynamics suggests an analysis of the transfer of energy between the various component motions that include the turbulent kinetic energy, and the mean polymeric and elastic potential energies. It is shown that the primary effect of the interaction between the turbulent and polymeric fields is to transfer energy from the turbulence to the polymer.

1. Introduction

Since the pioneering experiments by Toms [1], it is known that the addition of minute amounts of long polymer chains to organic solvents, or water, can lead to significant turbulent drag reduction. This discovery has had many practical applications such as in pipeline fluid transport, oil well operation, vehicles design and submersible vehicle projectiles, and more recently arteriosclerosis treatment. The numerical simulation of this phenomenon is more recent. The availability of high-performance computers has allowed direct numerical simulations (DNS) of polymer drag reduction flows from the mid-nineties. Sureshkumar *et al* [2] were the first to perform direct numerical simulations of drag

¹ To whom any correspondence should be addressed.



reduction with a viscoelastic fluid. They used the FENE-P model (Finitely Extensible Non-linear Elastic in the Peterlin approximation), appropriate for dilute polymer solutions. Afterwards, Dimitropoulos *et al* [3] performed a detailed analysis of the budget of kinetic energy and streamwise enstrophy for the FENE-P solution at low Reynolds number, and showed that the inhibition of vortex stretching was a possible mechanism responsible for drag reduction.

More recently, other DNS were carried out with the FENE-P fluid. Dubief *et al* [4] reproduced the low and high drag reduction regimes. At low drag reduction ($DR < 40\%$), the log law region is simply moved away from the wall. At high drag reduction, the log region is again moved away from the wall but its slope is increased with respect to the Newtonian flow. Dimitropoulos *et al* [5] considered the development of a zero-pressure-gradient flat plate turbulent boundary layer, later extending this study to inhomogeneous spatial distribution of polymer concentration [3]. It should be mentioned that while DNS has helped to provide more insight into the physics of polymer-turbulence interaction, the numerical workload required by viscoelastic DNS make them only amenable to relatively modest Reynolds numbers on large scale mainframe computers. From the engineering point of view, it is advantageous to envisage viscoelastic turbulent closure models for such flows. In this spirit, there have been recent attempts towards RANS (Reynolds Averaged Navier-Stokes) modeling. Such models have included zero-equation [6], one-equation [7], and two-equation $k-\epsilon$ [8] models.

From a phenomenological point of view, there exists a longstanding controversy between the two major theories which have been proposed to explain polymer drag reduction, and which still prevails in spite of the large amount of numerical data now available. Some authors [9,10,11] support Lumley's [12] viscous theory, which explains the phenomenon by an increase of the effective viscosity in the buffer layer. Others [13,14] gravitate around the elastic theory proposed by Tabor and De Gennes [15], which states that Kolmogorov's energy cascade is interrupted due to the elastic behavior of the polymer. We are convinced that studying viscoelastic turbulence may more generally lead to a better understanding of the physics of wall turbulence, in particular its self-sustaining mechanisms.

The presentation here will focus on the development of the FENE-P constitutive model followed by a discussion of the energetic exchange, based on DNS study at a friction Reynolds number of 1000, between the turbulent flow and polymeric fluid as represented by the FENE-P model.

2. Non-Newtonian and Viscoelastic Fluids

The theory of non-Newtonian and viscoelastic fluids flourished in the second half of the last century with the developments of (molten and dilute) polymers and the growth of materials science and engineering that generated many new products and applications. From a fluid and flow dynamic perspective, it is useful to provide a brief description of the hierarchy of such non-Newtonian and viscoelastic models. Modern constitutive equations have evolved by taking into account more and more of the microscopic features of polymeric fluids. The interplay between micro- and macro-scale is of importance and leads to a multi-scale approach towards the goal of incorporating more physics into the models that range from linear constitutive equations through to more sophisticated relationships. The theory of constitutive equations for non-Newtonian and viscoelastic fluids has been described in numerous books, and the reader is referred to the following references [16-23]. Of particular relevance is the recent text by Deville and Gatski [23] which serves as a guide for the model development remarks.

2.1. Mechanical models

At the introductory limit of non-Newtonian constitutive equations are the generalized Newtonian fluids. The constitutive equation for such fluids is generated by allowing the dynamic viscosity to depend on the shear rate $\dot{\gamma}$ such that $\mu = \mu(\dot{\gamma})$. A very common model is the power law

$$\mu(\dot{\gamma}) = K\dot{\gamma}^{m-1} \quad (2.1)$$

with K the consistency factor and m the index of the power law ($m = 1$, $K = \mu$ for the Newtonian case). For many polymers, blood or food liquids, m is between 0.3 and 0.6. Fluids with $m < 1$ are pseudo-plastic fluids; those with $m > 1$ are dilating fluids. The viscosity μ decreases with respect to increasing shear rate $\dot{\gamma}$ for a pseudo-plastic fluid so that the viscosity is shear thinning. In the opposite case, where μ increases with increasing $\dot{\gamma}$, the viscosity is shear thickening.

A slightly more complex constitutive equation describes so-called yield fluids. These fluids exhibit a yield stress. This means that the shear stress has to be higher than a threshold yield stress for the fluid to flow. Below this threshold, the fluid behaves like a solid, and above it may behave as Newtonian or power-law like. An example of such a fluid that occurs in our everyday lives is toothpaste. These yield fluids produce plug flows in channels or pipes since near the symmetry axis the shear stress vanishes and therefore does not reach the threshold value.

A characterizing trait of these generalized Newtonian models was the relationship between a function of the shear rate and shear stress. The next level of complexity involves not only the stress field but also a stress rate. The original concepts for the design of linear viscoelastic models were framed with the aid of mechanical parts involving springs and dashpots. A simple example illustrates the development of such a model. Consider a spring with constant stiffness k for the elastic part and a dashpot of viscosity μ . If these two mechanical elements are connected in series, the resultant stress is described by the Maxwell model. In a one-dimensional extensional flow, for example, the stress-strain relation for the spring is $\Sigma = k\epsilon_1$ and for the dashpot $\Sigma = \mu\dot{\epsilon}_2$. The strains ϵ_1 and ϵ_2 are respective measures of an extensional motion. The same stress (force), Σ , applied to the model generates a displacement Σ/k in the spring and a velocity Σ/μ in the dashpot. The total velocity is then

$$\dot{\epsilon} = \dot{\epsilon}_1 + \dot{\epsilon}_2 = \frac{\dot{\Sigma}}{k} + \frac{\Sigma}{\mu} \quad \text{or} \quad \Sigma + \lambda\dot{\Sigma} = \mu\dot{\epsilon} \quad (2.2)$$

where $\lambda = \mu/k$ is a characteristic time of the model and $\dot{\epsilon}$ is the strain rate. Note that if the stress strain relation is rewritten as

$$\frac{d}{dt}(\Sigma e^{t/\lambda}) = \left(\frac{\mu}{\lambda}\dot{\epsilon}\right)e^{t/\lambda} \quad (2.3)$$

and if the constraint that Σ remains finite when $t \rightarrow \infty$ is imposed, the integration in time yields [9]

$$\Sigma(t) = \int_{\tau=-\infty}^t \frac{\mu}{\lambda} \exp\left[-\frac{(t-\tau)}{\lambda}\right] \dot{\epsilon}(\tau) d\tau \quad (2.4)$$

with the quantity in the integrand,

$$G(t-\tau) = \frac{\mu}{\lambda} \exp\left[-\frac{(t-\tau)}{\lambda}\right] \quad (2.5)$$

called the relaxation modulus. This expression shows that in the Maxwell model the stress at the present time depends on the history of the deformation through the strain rate. In addition, the fluid possesses an intrinsic property of fading memory that gives more weight to the recent past than to the distant past, with the decay rate driven by the material relaxation time. The Newtonian case is recovered with $G = \mu\delta(t - \tau)$ and a linear elastic solid for $G = G_0$.

These relatively simple ideas can be generalized and comprise the group of constitutive equations of the rate type. Stress rate models like the Oldroyd-B fluid, used for dilute solutions are far from the industrial fluids of polymer type that offer shear-thinning viscosity, but are nevertheless satisfactory in many problems and form a fundamental building block of non-Newtonian modeling. It is assumed that the polymers are diluted in a Newtonian solvent so that the Cauchy stress tensor can be split into two parts

$$\boldsymbol{\Sigma} = -p\mathbf{I} + 2\mu_0\mathbf{S} + \boldsymbol{\Xi}_v \quad (2.6)$$

where the first part is the Newtonian solvent which consists of an isotropic part and a deviatoric part characterized by the viscosity μ_0 and rate of strain tensor \mathbf{S} , and the second part, the viscoelastic stress $\boldsymbol{\Xi}_v$. Now consider a similar generalization of the simple 1D Maxwell model given in (2.2) by replacing $\boldsymbol{\Sigma}$ with the stress $\boldsymbol{\Xi}_v$ and the strain rate \mathbf{S} . This yields a transport equation for $\boldsymbol{\Xi}_v$ given by

$$\boldsymbol{\Xi}_v + \lambda \frac{D\boldsymbol{\Xi}_v}{Dt} = 2\mu_1\mathbf{S} \quad (2.7)$$

In order to ensure the objectivity of (2.7), an objective stress rate needs to be introduced. The Oldroyd-B fluid constitutive equation is obtained by replacing the material time derivative of the extra-stress in (2.7) with the Oldroyd upper-convected derivative,

$$\boldsymbol{\Xi}_v + \lambda \overset{\nabla}{\boldsymbol{\Xi}}_v = 2\mu_1\mathbf{S} \quad (2.8)$$

or

$$\boldsymbol{\Xi}_v + \lambda \left(\frac{D\boldsymbol{\Xi}_v}{Dt} - \nabla\mathbf{v}\boldsymbol{\Xi}_v - \boldsymbol{\Xi}_v(\nabla\mathbf{v})^T \right) = 2\mu_1\mathbf{S} \quad (2.9)$$

where $\nabla\mathbf{v}$ is the solvent flow velocity gradient.

2.2. Dumbbell models

It has long been recognized that such mechanical models, formulated by assembling springs and dashpots, and simply using tensor generalizations to obtain corresponding multi-dimensional forms was inadequate. The latter day approach that developed was to base the model development on the nanoscale. However, it does not make sense to work at this level, especially since the intent is to design a model that is computationally tractable and efficient, and that takes some microstructure features into account. Fortunately, the complexity of the micro-macro description is reduced by a statistical mechanics argument. It is not intended here to be all inclusive in both detail and scope on the development of such models since there are a wide variety of viscoelastic models that have been developed (see [23] for a more inclusive list). The viscoelastic fluid model development will be limited polymeric fluids and to the FENE-P model for the viscoelastic/polymeric stress ($\boldsymbol{\Xi}_v = \boldsymbol{\Xi}_p$). This is the most popular model currently used in numerical simulations of viscoelastic turbulent flows.

The reader is referred to the numerous texts available on polymeric fluid dynamics for a more complete description of such model development (for example [16-23])

In general, a polymer chain may be composed of $N+1$ beads connected by N massless springs, each of length b as sketched in figure 1. The beads are assumed not to deform and may rotate with respect to each other with an end-to-end vector \mathbf{r} connecting bead 1 to bead $N+1$ at the ends of the chain.

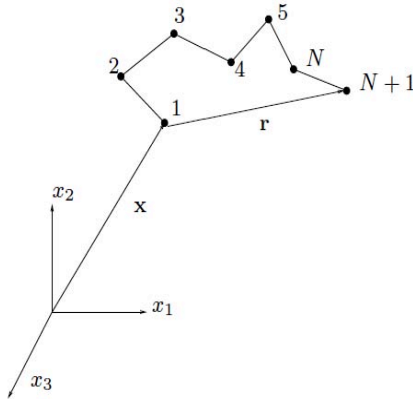


Figure 1. Polymer as chain of beads (from [23])

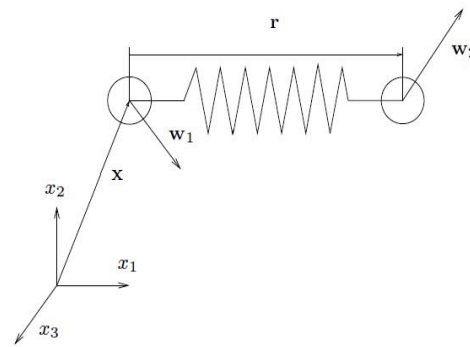


Figure 2. Elastic dumbbell (from [23])

The required interplay between the micro and macro behavior of polymeric chains can be represented by a Langevin equation for the vector connector \mathbf{r} containing the (macro) drag and friction forces and the (micro) Brownian forces,

$$\zeta \left[\frac{d\mathbf{r}}{dt} - (\nabla \mathbf{v}) \mathbf{r} \right] - \mathbf{f}_s = \mathbf{B} \quad (2.10)$$

where inertial forces have been assumed small, the local solvent velocity field is homogeneous with $\nabla \mathbf{v}$ the local velocity gradient, ζ ($= 6\pi\mu_s a$) is the friction coefficient associated with the Stokes drag on the beads (each of radius a), and the Brownian force is $\mathbf{B} = -n_p k_B \theta \partial \ln \psi / \partial \mathbf{r}$ with θ the absolute temperature. The probability density function $\psi(\mathbf{r}, t)$ is associated with the movement of the dumbbell and satisfies the Fokker-Planck equation,

$$\frac{\partial \psi}{\partial t} + (\nabla \mathbf{v}) \mathbf{r} \cdot \frac{\partial \psi}{\partial \mathbf{r}} - 2 \frac{k_B \theta}{\zeta} \frac{\partial^2 \psi}{\partial r^2} - \frac{2}{\zeta} \frac{\partial}{\partial \mathbf{r}} \cdot (\psi \mathbf{f}_s) = 0 \quad (2.11)$$

The Cauchy stress of the fluid is assumed to be an ensemble average over a volume \mathcal{V} that can be decomposed into the solvent volume \mathcal{V}_s , and the polymeric volume \mathcal{V}_p . The stress in the solvent part is the classical Newtonian stress involving the pressure, the rate of deformation tensor \mathbf{S} and the viscosity μ_s . These volume averages can also be represented by integration over the configuration space of the polymer using the pdf ψ .

The polymeric contribution to the stress is due to the drag force of the beads exerted on the solvent. As (2.10) shows, the drag force is balanced by the Brownian force and the nonlinear spring force so that the polymeric stress is then given by

$$\boldsymbol{\Xi}_p = \int (\mathbf{r} \otimes \mathbf{B}) \boldsymbol{\psi}(\mathbf{r}, t) d\mathbf{r} + \int (\mathbf{r} \otimes \mathbf{f}_s) \boldsymbol{\psi}(\mathbf{r}, t) d\mathbf{r} \quad (2.12)$$

where \otimes denotes the tensor product of two vectors. Since the *pdf* $\boldsymbol{\psi}$ vanishes on the polymer surface, the Brownian force contribution is isotropic and the resulting polymeric stress is

$$\begin{aligned} \boldsymbol{\Xi}_p &= -n_p k_B \boldsymbol{\theta} \mathbf{I} + n_p H f(\boldsymbol{\Xi}) \int (\mathbf{r} \otimes \mathbf{r}) \boldsymbol{\psi}(\mathbf{r}, t) d\mathbf{r} \\ &= -n_p k_B \boldsymbol{\theta} \mathbf{I} + n_p H f(\boldsymbol{\Xi}) \langle \mathbf{r} \otimes \mathbf{r} \rangle = -n_p k_B \boldsymbol{\theta} \mathbf{I} + n_p H f(\boldsymbol{\Xi}) \mathbf{c} \end{aligned} \quad (2.13)$$

where for the FENE-P model $f(\boldsymbol{\Xi})$ is the Peterlin function accounting for the nonlinear spring behaviour, $H (= 3k_B \boldsymbol{\theta} / Nb^2)$ is an entropic spring constant, n_p is the number density of polymer chains per unit volume, and $\mathbf{c} (= \langle \mathbf{r} \otimes \mathbf{r} \rangle)$ is the conformation tensor. Equation (2.13) is known as Kramers equation.

From (2.10) there remains one other contribution to the polymeric stress, that is, the drag force contribution. It is easier to evaluate this contribution to the stress by the polymeric chain by representing the complex chain by an elastic dumbbell model as shown in figure 2. The model corresponds to two spherical beads connected by either a nonlinear (entropic) spring. The single spring of the elastic dumbbell represents the net effect of the N springs of the polymer chain and the two beads represent the net effect of the $N+1$ beads of the chain with each bead moving with velocity $\mathbf{w}_{1,2}$. The contribution from the drag force to the polymer stress can be represented by

$$\begin{aligned} \boldsymbol{\Xi}_p &= n_p \zeta \int \left[\mathbf{r} \otimes \left(\frac{d\mathbf{r}}{dt} - (\nabla \mathbf{v}) \mathbf{r} \right) \right] \boldsymbol{\psi}(\mathbf{r}, t) d\mathbf{r} \\ &= \frac{n_p \zeta}{4} \left[\frac{d}{dt} \langle \mathbf{r} \otimes \mathbf{r} \rangle - (\nabla \mathbf{v}) \cdot \langle \mathbf{r} \otimes \mathbf{r} \rangle - \langle \mathbf{r} \otimes \mathbf{r} \rangle \cdot (\nabla \mathbf{v})^T \right] \\ &= \frac{n_p \zeta}{4} \frac{\delta \mathbf{c}}{\delta t} \end{aligned} \quad (2.14)$$

where $\delta / \delta t$ is the Oldroyd (upper convective) derivative. Its appearance is necessary to ensure that the polymeric stress tensor is objective. Equation (2.14) is known as the Giesekus equation. From (2.10), the contributions to the polymeric stress from the drag forces should balance those from the spring and Brownian forces. Thus, the polymeric stress contributions from (2.13) and (2.14) can be equated yielding an evolution equation for the conformation tensor

$$\lambda \frac{\delta \mathbf{c}}{\delta t} = -\frac{k_B \boldsymbol{\theta}}{H} \mathbf{I} + f(\boldsymbol{\Xi}) \mathbf{c} \quad (2.15)$$

where $\lambda = \zeta / (4H)$ is a relaxation time associated with the polymer chain. Equation (2.15) coupled with (2.13) provides the necessary mathematical formulation for the polymer chain motion and the polymeric stress link with the equations of fluid motion.

The Peterlin function, $f(\boldsymbol{\Xi}) = L^2 / (L^2 - \{\mathbf{c}\})$ where L is the maximum extension length of the polymer chain, is an important component in the interaction between the turbulent and polymeric

energies. (For the cases of interest in most DNS studies $L \sim O(10-10^2)$.) Before completing this section on the development of the FENE-P model, both the conformation evolution equation and polymeric stress equation can be non-dimensionalized with $k_B\theta/H$ for the conformation tensor \mathbf{c} and a rescaling of the conformation tensor to ensure that at equilibrium ($\delta\mathbf{c}/\delta t=0$) so that $\mathbf{c}=\mathbf{I}$ (see [24] for a thorough discussion of this rescaling). The final non-dimensional set of equations for the conformation tensor and polymeric stress tensor are given by

$$\lambda \frac{\delta\mathbf{c}}{\delta t} = -\mathbf{I} + f(\{\mathbf{c}\})\mathbf{c} \quad (2.16)$$

and

$$\mathbf{\Xi}_p = \frac{\mu_{p0}}{\lambda} [f(\{\mathbf{c}\})\mathbf{c} - \mathbf{I}] \quad (2.17)$$

where μ_{p0} is a polymeric viscosity such that $n_p k_B\theta \approx \mu_{p0}/\lambda$, and the Peterlin function is now redefined as

$$f(\{\mathbf{c}\}) = \frac{L^2 - 3}{L^2 - \{\mathbf{c}\}} \quad (2.18)$$

A consequence of this rescaling is the fact that at equilibrium $\mathbf{c}=\mathbf{I}$ so that $f(\{\mathbf{c}\})=1$ and $\mathbf{\Xi}_p=0$. The vast majority of studies done in connection with DNS of polymeric viscoelastic flows have utilized the FENE-P model. Such models are representative of nonlinear dumbbells, which preclude the infinite extendability of the linear dumbbell models represented by the Oldroyd-B fluids.

3. Numerical Simulations: Focus and Formulation

As with the case of Newtonian fluids, a primary motivation for using numerical simulations in the study of flow physics is the absence, or near-absence, of dynamic modeling. In the case of viscoelastic fluids, as the previous section showed, model development for the Cauchy stress introduced by the polymeric chains required careful consideration of the phenomenological behavior of a polymer chain. When such polymers are embedded in a turbulent flow, the multi-scale dynamics is quite complex. Until recently, and even today, the state-of-the-art is such that many aspects of the dynamic interchange between the turbulent flow stress fields and viscoelastic (polymeric) fluid stress fields is not completely understood.

The large majority of DNS studies of polymeric flows are performed in a fully developed channel flow. The obvious advantage is the simplification of boundary conditions and computational resources in both the streamwise and spanwise flow directions. This additionally enhances any spectral analysis of the flow dynamics since two directions can be Fourier analyzed. Fortunately such flows display a broad range of drag reduction (DR) features so there is no compromise from a dynamics standpoint.

Since such studies focus on the inner layer dynamics of the channel flow, wall scaling is usually used and is based on zero-shear rate variables with the length and time scaled by \mathbf{v}_{tot}/u_τ and $\mathbf{v}_{tot}/u_\tau^2$,

where $\mathbf{v}_{tot} = \mathbf{v}_s + \mathbf{v}_{p0}$ is the total zero-shear kinematic viscosity, and u_τ the friction velocity. In the following, standard notations for the channel flow geometry will be used, i.e. the channel streamwise direction is $x_1^+ = x^+$, the wall-normal direction is $x_2^+ = y^+$, and the spanwise direction $x_3^+ = z^+$, with the velocity field in the respective directions $(U^+, V^+, W^+) = (U_1^+, U_2^+, U_3^+)$.

Finally, in this section the notation will change from using matrix tensors and vectors to index notation, which will facilitate the presentation of material. Using this scaling, the dimensionless conservation equations are

$$\frac{\partial U_j^+}{\partial x_j^+} = 0 \quad (2.19)$$

$$\frac{DU_i^+}{Dt^+} = \frac{\partial U_i^+}{\partial t^+} + U_j^+ \frac{\partial U_i^+}{\partial x_j^+} = -\frac{\partial P^+}{\partial x_i^+} + \frac{\partial \Sigma_{ij}^+}{\partial x_j^+}, \quad (2.20)$$

with $\partial P^+ / \partial x^+$ the pressure gradient (this includes the constant non-zero contribution driving the flow as well as a time-dependent contribution), and the total stress tensor Σ_{ij}^+ being composed of (Newtonian) solvent and (polymeric) viscoelastic contributions

$$\Sigma_{ij}^+ = 2\beta_0 S_{ij}^+ + \Xi_{ij}^{p+} \quad (2.21)$$

Here, $S_{ij}^+ = (\partial U_i^+ / \partial x_j^+ + \partial U_j^+ / \partial x_i^+) / 2$ is the strain rate tensor, β_0 the ratio of the Newtonian viscosity \mathbf{v}_s to the total zero-shear viscosity \mathbf{v}_{tot} . For a FENE-P dumbbell model, the polymeric stress is given by (cf. (2.17))

$$\Xi_{ij}^{p+} = \alpha_0 \left[f(\{\mathbf{c}\}) c_{ij} - \delta_{ij} \right] \quad (2.22)$$

where $\alpha_0 = (1 - \beta_0) / We_{\tau_0}$, and with $We_{\tau_0} = \lambda u_\tau^2 / \mathbf{v}_{tot}$ the friction Weissenberg number representing the ratio of the elastic relaxation time λ relative to the viscous timescale. The polymeric stress for a FENE-P fluid includes the Peterlin function $f(\{\mathbf{c}\})$ that was defined in (2.18), ensuring shear-thinning behavior and a finite elongational viscosity for a finite value of the extension rate, with L the fully-stretched polymer length and $\{\mathbf{c}\}$ designating the trace of the conformation tensor \mathbf{c} . The equation system is closed with an evolution equation for \mathbf{c} (cf. (2.16))

$$\frac{Dc_{ij}}{Dt^+} = (c_{ik} S_{kj}^+ + S_{ik}^+ c_{kj}) - (c_{ik} W_{kj}^+ - W_{ik}^+ c_{kj}) - \frac{f(\{\mathbf{c}\}) c_{ij} - \delta_{ij}}{We_{\tau_0}}, \quad (2.23)$$

where $W_{ij}^+ = (\partial U_i^+ / \partial x_j^+ - \partial U_j^+ / \partial x_i^+) / 2$ is the rotation rate tensor.

For the results to be shown here, the simulation parameters are set as $\beta_0 = 0.9$ and $Re_{\tau_0} = 1000$, where $Re_{\tau_0} = u_\tau h / \mathbf{v}_{tot}$ (with h the channel half-width) is the zero-shear friction Reynolds number setting the turbulence level. Two drag reduction cases are studied: $L = 30$, $We_{\tau_0} = 50$, medium

percentage DR of 30%, and $L = 100$, $We_{\tau_0} = 115$, high percentage DR of 58%. The simulation details can be found in [11,25,26].

The Peterlin function can be related to the potential energy associated with the extension of the polymer molecule. The nonlinear spring force of a finitely extendable nonlinear elastic (FENE) polymer model was given in equation (2.13) and leads to a relation for the elastic potential energy given by

$$\mathcal{E}_p^+ - \mathcal{E}_{p0}^+ = \alpha_{0L} \ln[f(\{c\})] \quad (2.24)$$

where $\alpha_{0L} = \alpha_0(L^2 - 3)/2$, and \mathcal{E}_{p0}^+ is a constant reference energy at equilibrium (recall $\Xi^{p+} = 0$ at equilibrium). This yields for the Peterlin function the relation,

$$f(\{c\}) = e^{(\mathcal{E}_p^+ - \mathcal{E}_{p0}^+)/\alpha_{0L}} \quad (2.25)$$

and the polymeric stress

$$\Xi_{ij}^{p+} = \alpha_0 \left[e^{(\mathcal{E}_p^+ - \mathcal{E}_{p0}^+)/\alpha_{0L}} c_{ij} - \delta_{ij} \right] \quad (2.26)$$

The polymeric energy $\Xi_{ii}^{p+}/2$ is then directly linked to the exponential of the potential energy of the extended polymer.

4. Energetic Exchange

Although the primary focus in this section will be on the energetic exchange between the turbulent flow and the polymeric chain, it is useful to see the net effect on the mean flow at different DR levels. Figure 3 shows the mean velocity across the channel for both the 30% and 58% DR cases. At $Re_{\tau_0} = 1000$ a well-defined log-law region starts to appear (cf. [4,27]). When compared to the theoretical maximum drag reduction (MDR) limit [28], it is apparent that as Reynolds number and DR levels increase both the wall layer intercept and log-law slope change. It is this variation in the sublayer/buffer layers that has motivated much of the simulation studies to date.

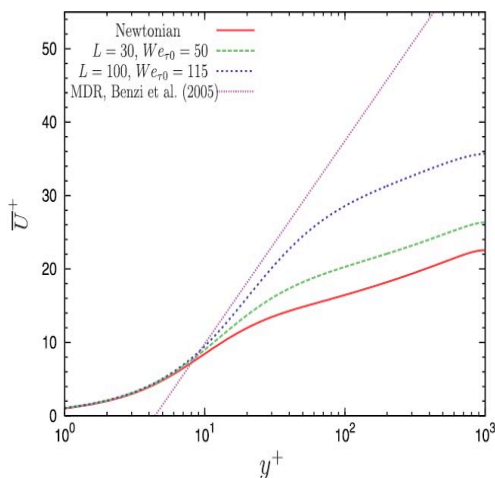


Figure 3. Mean velocity profiles for moderate and high drag reduction case (from [11])

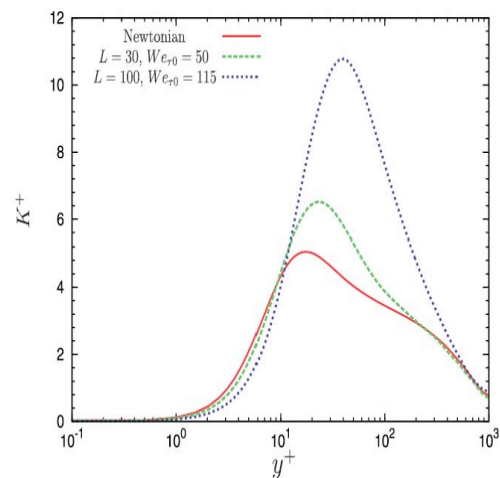


Figure 4. Turbulent kinetic energy for moderate and high drag reduction case (from [11])

As figure 4 shows, the turbulent kinetic energy K^+ peak level increases for viscoelastic flow relative to the Newtonian case. The figure further confirms the thickening of the sublayer since the peak of turbulent kinetic energy moves away from $y^+ \approx 17$ for the Newtonian fluid to $y^+ \approx 40$ for the high DR case. Explaining the increase in the turbulent kinetic energy level for viscoelastic flows is not that trivial. It is necessary to examine the dynamic balance associated with the turbulent kinetic equation given by

$$\begin{aligned} \frac{DK^+}{Dt^+} = & P_m^+ - \underbrace{\beta_0 \left(\frac{\partial u_i^+}{\partial x_k^+} \right)^2}_{\epsilon^+} + \underbrace{\beta_0 \frac{\partial^2 K^+}{\partial x_k^{+2}}}_{D_v^+} + \underbrace{\frac{\partial(\overline{p'^+ u_i'^+ \delta_{ik}})}{\partial x_k^+}}_{D_p^+} + \underbrace{\frac{\partial(\overline{u_i'^+ u_i'^+ u_k'^+ / 2})}{\partial x_k^+}}_{D_t^+} \\ & - \underbrace{\overline{\Xi'_{ik} p'^+ s'_{ki}}}_{P_{pt}^+} + \underbrace{\frac{\partial}{\partial x_k^+} (\overline{\Xi'_{ik} p'^+ u_i'^+})}_{D_{pt}^+} \end{aligned} \quad (3.1)$$

where $P_m^+ = -\tau_{ik}^+ \bar{S}_{ki}^+$ is the mean flow production. From the turbulent kinetic profiles for the Newtonian and viscoelastic cases shown in figure 4, the most significant change in the energetic balance should occur in the region $10 \leq y^+ \leq 60$ where the peak turbulent kinetic energy level is clearly set. As figure 5 shows, within this region the dynamics is dominated by the combination of diffusive transport and dissipation, namely $D_t^+ + D_v^+ - \epsilon^+$, with D_t^+ and D_v^+ both negative (although not shown growing in magnitude as viscoelasticity increases). Note that D_t^+ has the same magnitude as dissipation ϵ^+ at the location of peak production by the mean flow, $y^+ \approx 25$. Since D_t^+ and D_v^+ spatially redistribute and diffuse energy within the channel rather than act as ultimate energy sinks, this suggests that the relative influence of ϵ^+ as compared to production diminishes with increasing viscoelasticity. As such the peak turbulent energy level in the polymeric cases can reach a higher value than in the Newtonian case.

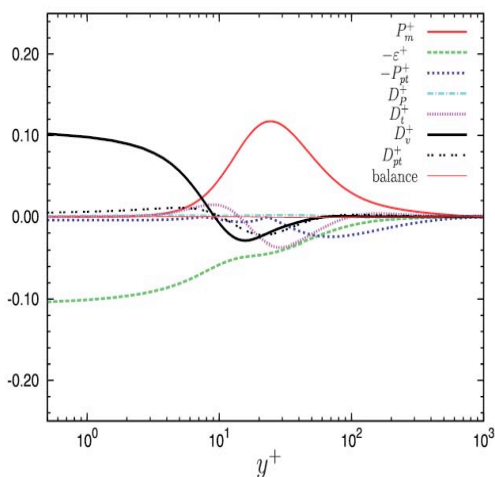


Figure 5. Turbulent kinetic energy budget for high drag reduction cases(from [11])

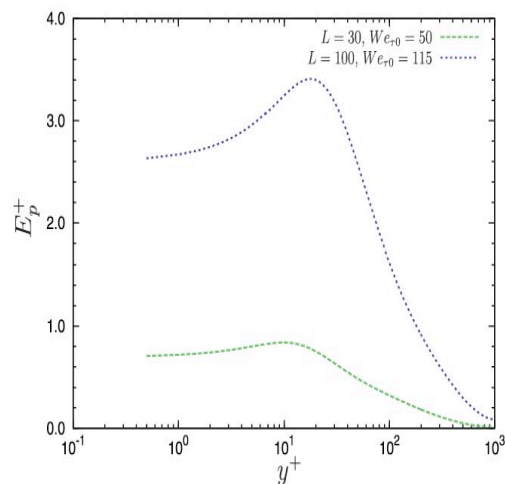


Figure 6. Elastic potential energy for moderate and high drag reduction case (from[11])

Figure 6 shows the mean elastic potential energy E_p^+ ($=\bar{\mathcal{E}}_p^+ - \mathcal{E}_{p0}^+$) for both the medium and high DR cases. In each case a maximum exists and is located at $y^+ \approx 12$ for medium DR and at $y^+ \approx 20$ for the high DR flow. Recall that the elastic potential energy is a direct consequence of the nonlinear spring force contribution to the polymer chain force balance. As such the peak in potential energy distribution for each DR case should correspond to the location of maximum polymer chain extension ($< L$) occurring within the channel. In addition, note that the relative peak amplitude between the two cases is a factor of 4. The fourfold increase in potential energy can be attributed to both the nonlinear behavior of the FENE-P spring (the Peterlin function) (see (2.24)), and the significant difference in the coefficient α_{0L} between the medium ($\alpha_{0L} = 0.9$) and high ($\alpha_{0L} = 4.5$) DR cases.

Since the polymeric stress (energy) is composed of the nonlinear spring force contribution and the (isotropic) Brownian motion contribution, the cross-channel distribution of the polymeric kinetic energy should be qualitatively similar to the potential energy distribution. This is shown in figure 7 for the mean polymeric energy, $K_p^+ = \bar{\Xi}_{ii}^{p+} / 2$. The polymeric energies for both DR cases are larger than the corresponding potential energy. The increase is due to the exponential relationship between polymeric stress and elastic potential energy given in (2.26) as well as the difference between α_0 for the medium ($\alpha_0 = 2.0 \times 10^{-3}$) and high ($\alpha_0 = 0.9 \times 10^{-3}$) DR cases. It is interesting to observe that the turbulent kinetic energy shown in figure 4 reaches a peak value of ≈ 6 at medium DR, and a peak value of ≈ 10 at high DR. This implies that for high DR the polymeric energy and the turbulent kinetic energy are of same order of magnitude; whereas, for medium DR the turbulent kinetic energy clearly dominates the polymeric energy. This means that as DR increases the polymer takes a proportionally larger amount of energy from the turbulent kinetic energy.

The polymeric energy equation is given by

$$\begin{aligned} \frac{DK_p^+}{Dt^+} = & P_{pm}^+ + P_{pt}^+ - \underbrace{\frac{f(\{\bar{\mathcal{C}}\})K_p^+}{We_{\tau_0}}}_{\boldsymbol{\varepsilon}_p^+} \\ & + \underbrace{f(\{\bar{\mathcal{C}}\}) \left[\left(\frac{\bar{\Xi}'_{ik}{}^{p+}}{f'(\{\bar{\mathcal{C}}\})} \right) \bar{S}_{ki}^+ + \bar{\Xi}_{ik}^{p+} \left(\frac{S_{ki}^+}{f'(\{\bar{\mathcal{C}}\})} \right) + \left(\frac{\bar{\Xi}'_{ik}{}^{p+} S_{ki}^+}{f'(\{\bar{\mathcal{C}}\})} \right) \right]}_{P_{pf}^+} \\ & - \underbrace{f(\{\bar{\mathcal{C}}\}) \frac{\partial}{\partial x_j} \left[\frac{u_j^+ K_p^+}{f(\{\bar{\mathcal{C}}\})} + \left(\frac{u_j^+ K_p^+}{f'(\{\bar{\mathcal{C}}\})} \right) + \left(K_p^+ + \frac{3\alpha_0}{2} \right) \left(\frac{u_j^+}{f'(\{\bar{\mathcal{C}}\})} \right) \right]}_{D_{pf}^+} \end{aligned} \quad (3.2)$$

where $P_{pm}^+ = \bar{\Xi}_{ik}^+ \bar{S}_{ki}^+$ is the production from mean shear. The corresponding cross-channel balance of each term is shown in figure 8. The dominant balance for the polymeric energy in the inner layer ($y^+ \lesssim 15$) is between the production due to mean shear, P_{pm}^+ , and the dissipation rate, $\boldsymbol{\varepsilon}_p^+$. The remaining sinks of energy in the overall polymeric energy balance in the inner and buffer layers are from the terms that are directly dependent on the mean and fluctuating components of the Peterlin function, P_{pf}^+ and D_{pf}^+ ,

where the latter contribution clearly dominates. In the outer layer ($y^+ \gtrsim 50$), the balance is between the turbulent exchange term P_{pt}^+ and the mean dissipation.

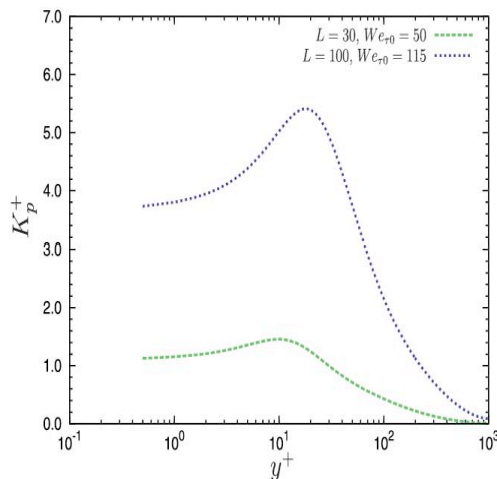


Figure 7. Polymeric kinetic energy profiles for high drag reduction case (from [11])

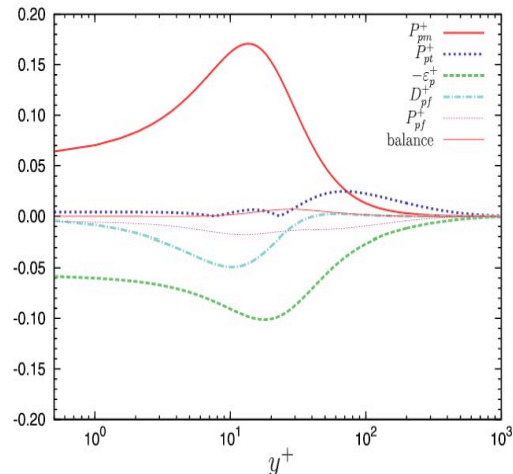


Figure 8. Polymeric energy budget for high drag reduction case (from [11])

5. On the Drag Reduction Mechanism

As the energetic budgets show, the polymer-turbulence interaction is governed by the turbulent exchange term P_{pt}^+ . As figure 8 shows, this term is predominantly positive so that the primary effect of the interaction between the turbulent and polymeric fields is to transfer energy from the turbulence to the polymer. For comparison, figure 9 shows the polymeric energy budget for the low drag reduction case. Note that the magnitude of the exchange term does not change between the low and high drag reduction cases. This one-way transfer, with an amplitude independent of the drag reduction regime, is

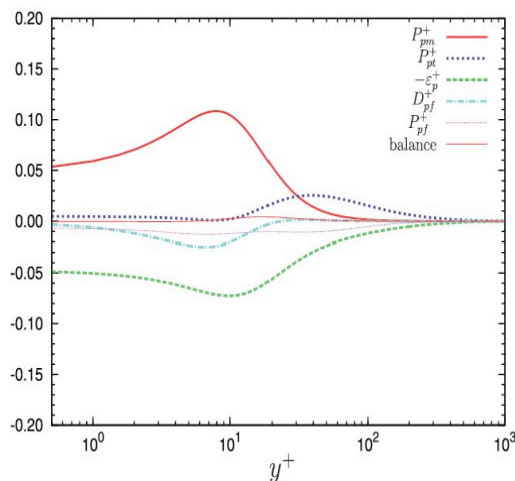


Figure 9. Polymeric energy budget for low drag reduction case (from [11])

in contradiction with the purely elastic coupling which is implicit within the elastic theory of the polymer drag reduction phenomenon by Tabor and De Gennes [15]. The elastic scenario indeed implies a two-way coupling where the exchange term would change sign, and would vary in magnitude with different elasticity levels.

6. Summary and Perspectives

Although in the limited space available it was not possible to pursue many of the aspects of viscoelastic fluid flows in detail, it is hoped that the material presented has provided an overview of the development of a commonly used and relatively accurate polymeric fluid stress constitutive equation – the FENE-P model. With this background in model development it is easier to see how the energetic exchange between the turbulent flow and

energetic exchange that depends on the distance from the bounding solid surface of the channel. Additional insight could also be obtained from a spectral analysis of the energy cascade and which could provide further information relative, not only, to spatial location but also on relevant spectral scales in the cascade.

Acknowledgments

This research has granted access to the HPC resources of [CCRT /CINES /IDRIS] under the allocation i20142b2277 made by GENCI (Grand Equipement National de Calcul Intensif). The data used herein was produced on the IBM Blue Gene/P computer *Babel* at the IDRIS/CNRS computing center, Orsay, France. Cross-channel statistics from the DNS database can be publicly accessed on-line at <http://lml.univ-lille1.fr/channeldata/>

7. References

- [1] Toms B A 1949 Some observations on the flow of linear polymer solutions through straight tubes at large Reynolds numbers Proc. of the 1st International Congress of Rheology vol 2 pp 135-141
- [2] Sureshkumar R, Beris A N and Handler R A 1997 Direct numerical simulation of the turbulent channel flow of a polymer solution *Phys. Fluids* **9** 743-755
- [3] Dimitropoulos C D, Dubief Y, Shakfeh E S G and Moin P 2006 Direct numerical simulation of polymer-induced drag reduction in turbulent boundary layer flow of inhomogeneous polymer solutions *J. Fluid Mech.* **566** 153-162
- [4] Dubief Y, White C M, Terrapon V E, Shakfeh E S G, Moin P and S. K. Lele S K 2004 On the coherent drag-reducing and turbulence-enhancing behaviour of polymers in wall flows *J. Fluid Mech.* **514** 271-280
- [5] Dimitropoulos C D, Dubief Y, Shakfeh E S G, Moin P and Lele S K 2005 Direct numerical simulation of polymer-induced drag reduction in turbulent boundary layer flow *Phys. Fluids* **17** 0105
- [6] Li C-F, Gupta V K, Sureshkumar R and Khomami B 2006 Turbulent channel flow of dilute polymeric solutions: drag reduction scaling and an eddy viscosity model *J. Non-Newton. Fluid* **139** 177-189
- [7] Pinho F T, Sadanandan B and Sureshkumar R 2008 One Equation Model for Turbulent Channel Flow with Second Order Viscoelastic Corrections *Flow Turbul. Combust.* **81** 337-367
- [8] Resende P R, Kim K, Younis B A, Sureshkumar, R and Pinho F T 2011 A FENE-P $k-\epsilon$ turbulence model for low and intermediate regimes of polymer-induced drag reduction *J. Non-Newton. Fluid* **166** 639-660
- [9] Benzi R 2010 A short review on drag reduction by polymers in wall bounded turbulence *Physica D* **239** 1338-1345
- [10] Procaccia I, L'vov V S and Benzi R 2008 Colloquium: Theory of drag reduction by polymers in wall-bounded turbulence *Rev. Mod. Phys.* **80** 225-247
- [11] Thais L, Gatski T B and Mompean G 2013 Analysis of polymer drag reduction mechanisms from energy budgets *Int. J. Heat Fluid Flw.* **43** 52-61
- [12] Lumley J L 1969 Drag reduction by additives *Annu. Rev. Fluid Mech.* **1** 367-384
- [13] Min T, Yoo J Y, Choi H and Joseph D D 2003 Drag reduction by polymer additives in a turbulent channel flow *J. Fluid Mech.* **486** 213-238
- [14] Dallas V, Vassilicos J C and Hewitt G F 2010 Strong polymer-turbulence interactions in viscoelastic turbulent channel flow *Phys. Rev. E* **82** 066303
- [15] Tabor M and de Gennes P G 1986 A cascade theory of drag reduction *Europhys. Lett* **7** 519-522
- [16] Bird R B, Armstrong R C and Hassager O 1987 *Dynamics of Polymeric Liquids. Vol. 1: Fluid Mechanics* (New York: Wiley)
- [17] Bird R B, Armstrong R C and Hassager O 1987 *Dynamics of Polymeric Liquids. Vol. 2: Kinetic Theory* (N York: Wiley)

- [18] Larson R 1988 *Constitutive Equations for Polymer Melts and Solutions* (Boston, Butterworth))
- [19] Joseph D D 1990 *Fluid Dynamics of Viscoelastic Liquids* (Berlin, Springer)
- [20] Huilgol R R and Phan-Thien N 1997 *Fluid Mechanics of Viscoelasticity* (Amsterdam, Elsevier)
- [21] Truesdell C and Rajagopal K R 2000 *An Introduction to the Mechanics of Fluids* (Boston, Birkhauser)
- [22] Phan-Thien N 2002 *Understanding Viscoelasticity Basics of Rheology* (Berlin, Springer)
- [23] Deville M O and Gatski T B 2012 *Mathematical Modeling for Complex Fluids and Flows* (Heidelberg, Springer)
- [24] Beris A N and Edwards B J 1994 *Thermodynamics of Flowing Systems with Internal Microstructure* (NewYork, Oxford)
- [25] Thais L, Tejada-Martinez A E, Gatski T B and Mompean G 2010 Temporal large eddy simulations of turbulent viscoelastic drag reduction flows *Phys. Fluids* **22** 013103
- [26] Thais L, Gatski T B and Mompean G 2011 A massively parallel hybrid scheme for direct numerical simulation of turbulent viscoelastic channel flow *Comput. Fluids* **43** 134-142
- [27] Housiadas K D and Beris A N 2006 Extensional behavior influence on viscoelastic turbulent channel flow. *J. Non-Newton. Fluid* **140** 41-56
- [28] Benzi R, De Angelis E, L'vov V S and Procaccia I 2005 Identification and calculation of the universal asymptote for drag reduction by polymers in wall-bounded turbulence *Phys. Rev. Lett.* **95** 194502